

A statistic study on raspberry vesicles: Formation and properties

Y. Guo^a, L. di Mare^b, J.S.S. Wong^{c,*}

^a School of Science, Qingdao University of Technology, Qingdao, 266520, China

^b St John's College, Oxford Thermofluids Institute and Department of Engineering Science, University of Oxford, Oxford, OX2 0ES, UK

^c Department of Mechanical Engineering, Imperial College London, London, SW 7 2AZ, UK

ARTICLE INFO

Keywords:

Polymer vesicles

Self-assembly

Dissipative particle dynamics simulations

ABSTRACT

This paper gives a statistic study on the formation of ABC raspberry vesicles under bulk swelling with DPD simulations. All vesicles formed through a disc wrap-up process, i.e. a disc micelle wraps up to form a vesicle. The lifetimes of the disc micelles before they become vesicles can be characterized as short and long (t_{fast} and t_{slow}). Vesicles formed with t_{fast} have a high loading efficiency and a wide size distribution. Most of them have low membrane permeability. They resist structural deformation under shear due to their high bending rigidity. Vesicles formed with t_{slow} have a narrow size distribution. They are small, and have low loading efficiency. A large portion of them have permeable membranes with low bending rigidity and structural defects. Shear could restructure these vesicles, and hence modify their permeability. Adjusting the repulsion between solvophobic polymers and solvents impacts on lifetimes of disc micelles. A reduction in such repulsion favours t_{slow} . The knowledge obtained can be used to design raspberry vesicles of desired size, loading and cargo release properties.

1. Introduction

Polymer vesicles (vesicles from here onwards) are hollow structures made of polymeric layers, which consist of hydrophobic membrane and hydrophilic shells. They are commonly formed by self-assembly of amphiphilic block copolymers in selective solvents. Vesicles with various structural features and properties have been achieved by polymers with different characteristics [1–3]. Cargos such as drugs, enzymes, dyes and reactive agents can be encapsulated by vesicles during vesicle formation. These cargos can then be released under specific conditions, depending on pH, light, shear [4–6]. Compared with lipid vesicles, polymer vesicles are more stable and robust under severe physical and chemical conditions [7]. As a result, polymer vesicles are potential cargo carriers for medical and biotechnological applications.

The permeability of a vesicle membrane affects the ability of a vesicle to isolate cargo effectively from its environment [14]. In most applications [8–11], unintentional leak should be prevented. Other applications may require carriers with more permeable membranes, enabling the possibility for core/shell transport [12,13]. One may introduce membrane channels to facilitate *trans*-membrane transport [15,16]. Vesicle permeability could also be controlled by the stimuli-responsive block copolymer on the membrane [17,18]. Shear can be an effective way to modify vesicle structure and regulate membrane permeability. Färber

et al. [19] found that shear force could induce a phase change of the membrane of giant unilamellar thermo-responsive vesicles, which increase the membrane permeability.

In bulk swelling, polymers are directly dissolved in water to form nanostructures without adding organic solvents [20,21]. However, the structures obtained via this route usually possess structure defects and/or broad size distributions [7,22,23]. The size and size distribution of vesicles may partly determine the fate of a vesicle for bio-related applications [24], as well as its cargo loading capacity. Ratamero et al. [25] studied analytically the maximum capacities of intracellular vesicles of four typical cargoes. They found the maximum capacity and the radius of a vesicle follows a second-order polynomial form.

To produce vesicles with a narrow size distribution, various preparation methods have been developed [26–29]. However, why a wide vesicle size distribution happens under bulk swelling is still unknown. Previous work has shown that vesicle mainly formed through two mechanisms [30]. In mechanism I, which is most common, vesicles formed through wrapping up of lamellar micelles. In mechanism II, vesicles formed through the nucleation and growth path. In this work, we would like to answer the following:

- 1) which vesicle formation mechanism dominates under bulk swelling; and

* Corresponding author.

E-mail address: j.wong@imperial.ac.uk (J.S.S. Wong).

<https://doi.org/10.1016/j.polymer.2023.126058>

Received 17 March 2023; Received in revised form 21 May 2023; Accepted 22 May 2023

Available online 24 May 2023

0032-3861/© 2023 The Authors. Published by Elsevier Ltd. This is an open access article under the CC BY license (<http://creativecommons.org/licenses/by/4.0/>).

2) the impact of formation process on the properties of the vesicles.

In this study, raspberry vesicles are used as model vesicles. They are hollow structures whose surfaces are decorated by physically or chemically distinct domains. Raspberry vesicles have recently been used to study the effect of varying surface roughness on Pickering emulsifier performance [31]. Compared to vesicles with homogenous membranes, we recently found [32] raspberry vesicle achieves high cargo release rates under wall shear at shear rates similar to those encountered in a tribological contact. Hence these vesicles can potentially be used for engineering applications. However, there still lacks a systematically study on these vesicles.

Dissipative particle dynamics (DPD) simulations were performed to follow a large group of raspberry vesicles self-assembled from star terpolymers. Their formation paths under bulk swelling were examined. The effect of formation path on vesicle properties, including size distribution, encapsulation efficiency and permeability, were investigated. In particular, this paper explored the effect of shear on the release properties of vesicles growing via bulk swelling.

2. Methodology

The self-assembly of amphiphilic star terpolymers was monitored using dissipative particle dynamics (DPD) simulation [33]. In the simulation, polymer chains are coarse-grained to chains composed of DPD beads of equal size. The motion of DPD particles is governed by Newton's equation of motion. The pair-wise force acting on particle i includes conservative force \vec{F}_{ij}^C , dissipative force \vec{F}_{ij}^D , and random force \vec{F}_{ij}^R . The conservative force \vec{F}_{ij}^C is a soft-repulsive force and is given by

$$\vec{F}_{ij}^C = \begin{cases} a_{ij}(1 - r_{ij}/r_c)\hat{r}_{ij} & (r_{ij} < r_c) \\ 0 & (r_{ij} \geq r_c) \end{cases} \quad (1)$$

where $\vec{r}_{ij} = \vec{r}_i - \vec{r}_j$, $r_{ij} = |\vec{r}_{ij}|$, $\hat{r}_{ij} = \vec{r}_{ij}/|\vec{r}_{ij}|$, a_{ij} is the maximum repulsion between beads i and j , r_c is the cut-off distance between two particles with value 1.0. A spring force \vec{F}_{ij}^S has been introduced between adjacent polymer beads to simulate polymer chains. It follows a simple harmonic potential with a spring constant set at 25.0.

Two model systems are set up. They both consist of block star terpolymers made of A-, B- and C- beads in a solvent S. B-beads are solvophilic, while A- and C-beads are solvophobic. The interaction parameters a_{ij} chosen [34] for the first model system are shown in Table 1. In this case, A-, B- and C-blocks correspond to poly (ethylene), poly (ethylene oxide), and poly (perfluoropropylene oxide) in water S. As a result, A, B, and C blocks segregate into distinct nano-domains. This system has $a_{CS} = 125$ and is labelled as ABC-125. The second model system, referred as ABC-100, has $a_{CS} = 100$. This allows the effect of the interaction between polymer and the solvent on vesicle formation to be investigated.

Star terpolymer $A_{12}B_6C_2$ (7680 chains in total) were added in solvent S with a polymer volume concentration $\phi_p = 10\%$ in a periodic box of size $80.0r_c \times 80.0r_c \times 80.0r_c$ ($112 \times 112 \times 112 \text{ nm}^3$) from an initially homogeneous state. Thus, we had 1,536,000 beads in one box. The simulations were conducted under NVT ensemble. The time step was Δ

$t = 0.04$ for all simulations. Six different initial configurations were studied for each model system. In total, 23 and 20 vesicles were examined for ABC-125 and ABC-100 respectively.

Bulk shear was applied to investigate the structure stability and cargo release behavior of vesicles. Shear was applied by changing the shape of the simulation box during the dynamics run. A constant strain rate $\dot{\gamma} = 1 \times 10^8 \text{ s}^{-1}$ has been applied. The strain is defined as offset divided by the length, where the length is the initial box length in the direction perpendicular to shear (i.e. the z box length for xz deformation), and the offset is the change in the shear direction (i.e. the change in the x box length for xz deformation) [[32]].

3. Results and discussion

3.1. Formation of raspberry vesicles

Amphiphilic star terpolymer $A_{12}B_6C_2$ self-assembles to various structures in solvent S. Note that A- and C-beads are solvophobic, while B-beads are solvophilic. Fig. 1 shows how these structures in ABC-125 evolve with time. Polymer chains are randomly distributed in the solvent at time $t = 0$ (Fig. 1a). They coalesce into small micelles (parent micelles) which then collide and merge to form bigger micelles (daughter micelles), see Fig. 1b. These daughter micelles have various shapes, for example, a disc micelle is highlighted in Fig. 1c. These micelles continue to merge and some of them eventually become vesicles (Fig. 1d). As the simulation continues, more vesicles are formed (Fig. 1e).

There are many ways a group of micelles could merge and form a vesicle. One formation path is illustrated by following the formation of a vesicle, highlighted in Fig. 2a0 with a dashed circle. It originated from two micelles, that merged and eventually formed a vesicle (Fig. 2a1 – 2a6).

The shape of an aggregate can be characterized by its principal moments of inertia with respect to its centre of mass, I_{xx} , I_{yy} , I_{zz} (see definition in inset in Fig. 3d). Typically, a spherical aggregate will have normalised principle moments of inertia $\frac{I_{yy}}{I_{xx}}$ and $\frac{I_{zz}}{I_{xx}} \approx 1$, while $\frac{I_{yy}}{I_{xx}} < \frac{I_{zz}}{I_{xx}}$ and $\frac{I_{yy}}{I_{xx}} \approx \frac{I_{zz}}{I_{xx}} > 1$ correspond to a cylinder and a disk respectively. The evolutions of $\frac{I_{yy}}{I_{xx}}$ and $\frac{I_{zz}}{I_{xx}}$ of the highlighted vesicle in Fig. 2a0 are presented in Fig. 3a, various stages of evolution corresponding to the snap shots in Fig. 2 are labelled. Two micelles (parent micelles) touch at $t - t_{merge} = 0$ and form a daughter micelle, which is an elongated, cylindrical structure ('a2', see also Fig. 2a2). This daughter micelle rapidly re-structures ('a3', see also Fig. 2a3) and eventually forms a disk ('a4', see also Fig. 2a4). The disk micelle remains for a while ('a4' in Fig. 3a). It then curls up ('a5', see also Fig. 2a5) and finally closes to form a spherical vesicle ('a6', see also Fig. 2a6). In this case, the vesicle is formed through a disk micelle closure process, a common path reported in the literature as Mechanism I.

The stages of vesicle formation highlighted in Fig. 2 are representative of vesicles formed by ABC-125 and ABC-100. In fact, all vesicles in this study are formed through a disk micelle closure process although the lifetime of disk micelles varies. The distribution of the lifetime of disk micelles could be found in Fig. S1. In order to better describe the properties of the vesicles, two groups of vesicles can be identified based on the lifetime of the disk micelles. Group 1 vesicles (Fig. 3b and d) undergo fast transition with the lifetime of the disk micelle < 500000 timesteps (t_{fast}) while Group 2 vesicles (Fig. 3a and c) experience slow transition with lifetime of the disk micelle > 500000 timesteps t_{slow} . For ABC-125, 83% vesicles belong to Group 1 while 17% Group 2. For ABC-100, 60% of the vesicles are Group 1 and 40% Group 2. Thus lower a_{CS} promotes the vesicle formation with t_{slow} .

The formation of a spherical vesicle is driven by the desire to reduce the surface area of an aggregate. Assuming the volume of an aggregate V after merging from parent micelles remains constant during the vesicle

Table 1
Interaction energy parameters.

Interaction parameter, a_{ij} (in DPD units)	A	B	C	S (Water)
A	25.0			
B	38.5	25.0		
C	78.0	89.4	25.0	
S	97.9	26.0	100.0–125.0	25.0

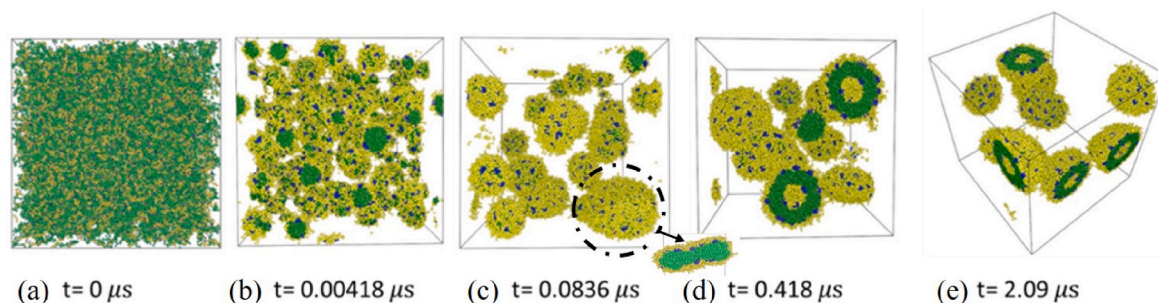


Fig. 1. Self-assembly observed in ABC-125. Green, yellow, and blue beads correspond to A-, B- and C-beads respectively. Solvent beads are omitted for clarity. A disc micelle, together with its cross-section, is highlighted in (c). (For interpretation of the references to colour in this figure legend, the reader is referred to the Web version of this article.)

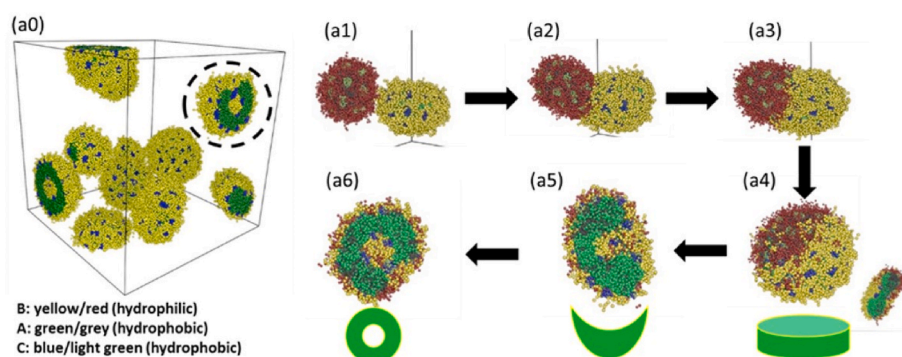


Fig. 2. Evolution from two micelles collision to vesicle. Different colour beads for the two vesicles are used in Figures a2-a6 to show that mixing of polymer chains from both micelles occurs. The colour codes for A-, B-, C- in micelle 1 are green, yellow and blue, while the colour codes for A-, B-, C- in micelle 2 are grey, red and light green. Schematics in a4 – a6 shows the structures of aggregates. (For interpretation of the references to colour in this figure legend, the reader is referred to the Web version of this article.)

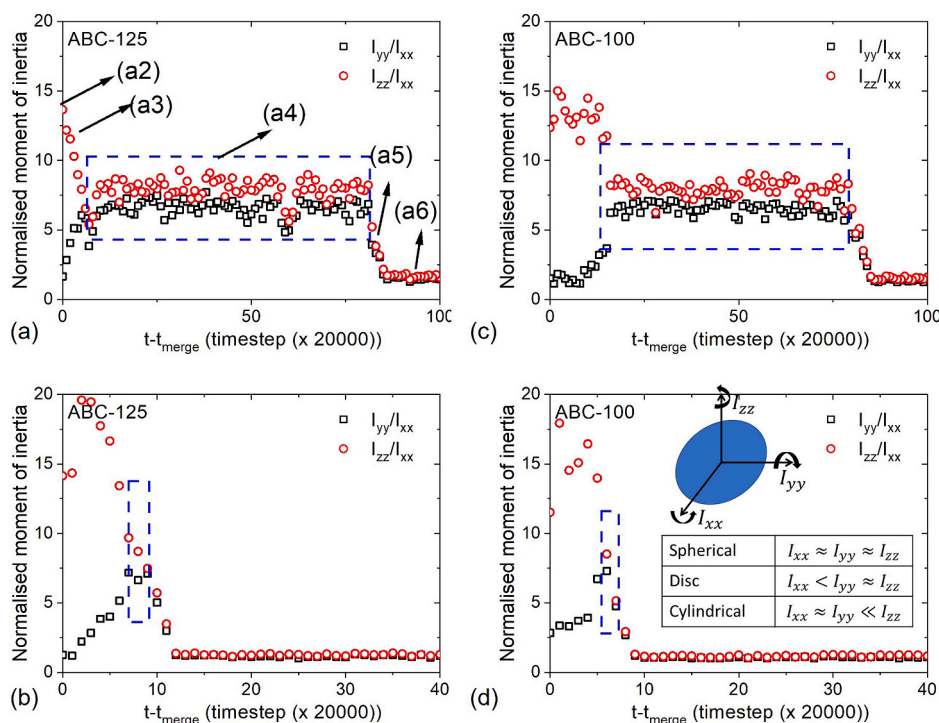


Fig. 3. Evolution of geometry of aggregates monitored by their normalised moment of inertia. A narrower time range is used in Fig. S2 in the supplementary information. For ABC-125: vesicles formed with (a) slow transition (long t_{disk} , Group 2 vesicles); (b) fast transition (short t_{disk} , Group 1 vesicles). For ABC-100: vesicles formed with (c) slow transition (long t_{disk} , Group 2 vesicles); (d) fast transition (short t_{disk} , Group 1 vesicles). I_{xx} , I_{yy} , I_{zz} are principal moments of inertia of the aggregate with respect to its centre of mass. Note labells in (a) correspond to various stages of the aggregate as shown in Fig. 2.

formation process, the surface area A of an aggregate normalised by $\sqrt[3]{V^2}$, A_n , can be estimated by $A_n = 0.95 \left(\frac{2}{R_n} + 2\pi R_n^2 \right)$, where R_n is the radius of an aggregate normalised by $\sqrt[3]{V}$. The predictions are shown as black dash lines and are compared with computational results for each

vesicle, see Fig. 4. Each symbol type is for one aggregate which eventually forms a vesicle. Regardless of a_{CS} (ABC-125 for Fig. 4a and b; and ABC-100 for Fig. 4c and d), three clusters of data points can be found. The data reflect that the aggregates transform from an elongated micelle (Stage 1) to a disk micelle (Stage 2), then finally to a spherical

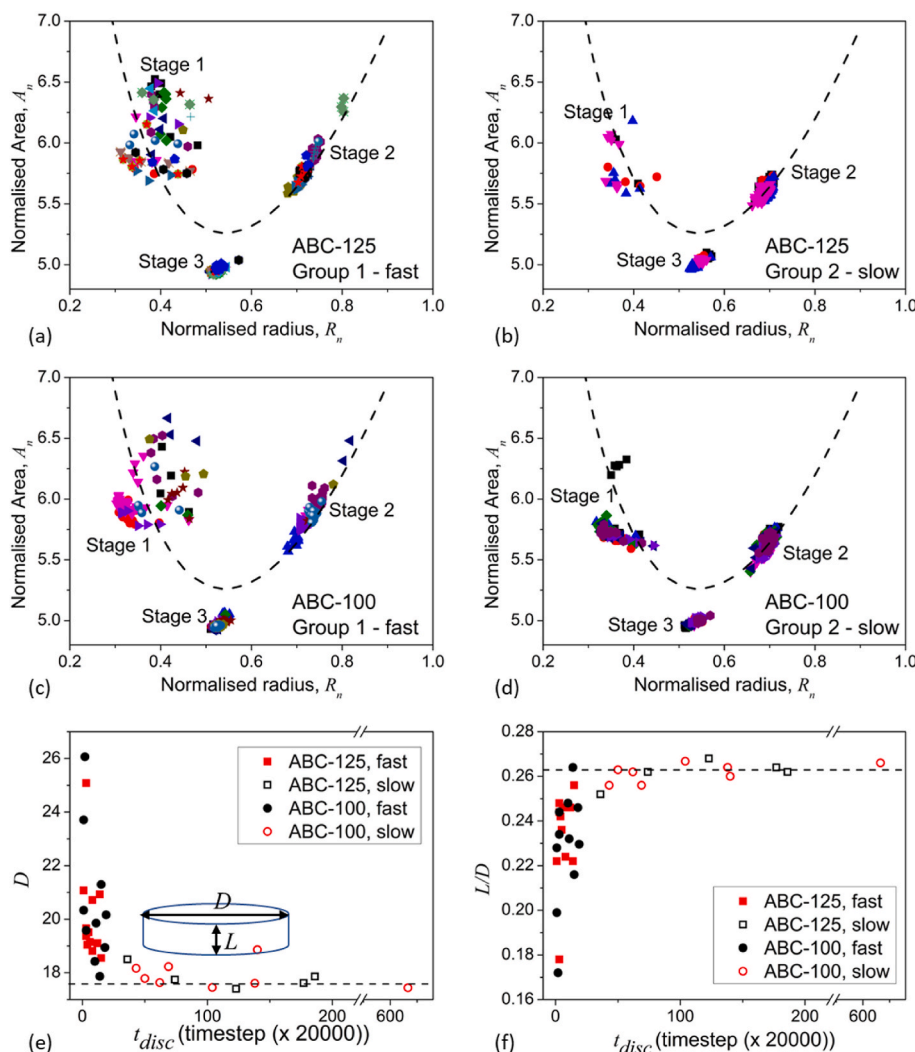


Fig. 4. Normalised surface area A_n as a function of normalised radius of the aggregate R_n . For ABC-125 (a) Group 1 –with t_{fast} ; (b) Group 2 – with t_{slow} . For ABC-100 (c) Group 1 – with t_{fast} ; (d) Group 2 –with t_{slow} . Assuming V is constant, the dash lines are the theoretical prediction, $A_n = 0.95 \left(\frac{2}{R_n} + 2\pi R_n^2 \right)$. Each symbol type represents an aggregate that becomes a vesicle. The relationship between (e) diameter D of a disc micelle in Stage 2 and its lifetime t_{disc} ; and (f) L/D and t_{disc} , assuming these micelles are circular discs.

(Stage 3) as time progresses. The predictions (the dash lines) and the observations match relatively well.

Large scatter of data points around predicted values is observed in Stage 1. This is due to the diverse elongated structures of daughter micelles which emerged from parent micelles of large variation of size and geometry. These elongated micelles gradually evolve to disks (stage 2), whose surface areas follow closely to predictions. In stage 3, spherical

vesicles are formed. They have the lowest area A_n , and are most energetically favourable compared to the disc and cylindrical micelle. Area for spherical micelles is lower than predicted values. This is due to the formation of an inner cavity in an aggregate (hence, a vesicle).

As daughter micelles transform to disc micelles, discs with t_{fast} (Group 1, Fig. 4a and c) have a larger range of R_n , higher average R_n and higher A_n , as compared to those with t_{slow} (Group 2, Fig. 4b and d).

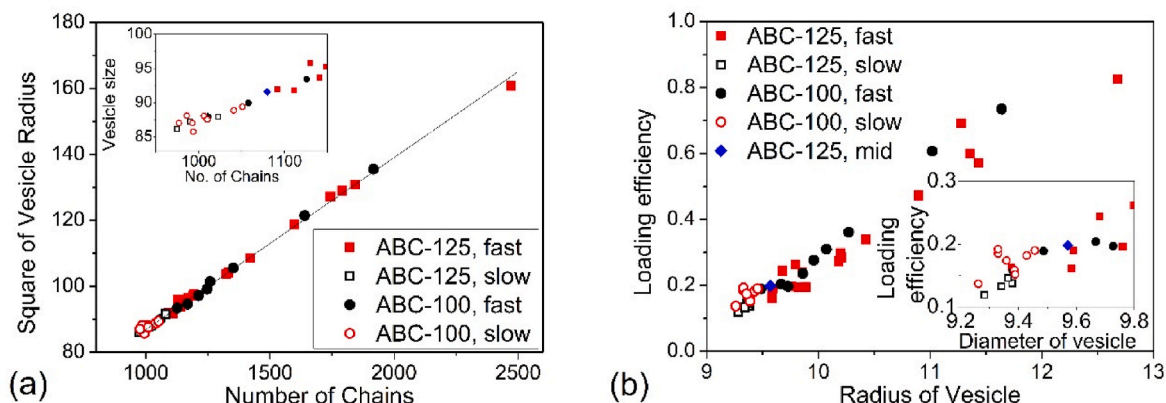


Fig. 5. The relationship between (a) square of vesicle radius and number of chains of a vesicle and (b) the loading efficiency and the radius of a vesicle. Insets focus on results from small vesicles. Vesicles formed by Group 1 (t_{fast}) and Group 2 disc micelles (t_{slow}) are shown as solid and open symbols.

Approximating these disc micelles as circular discs, the relationship between the diameter of a disc micelle D and its lifetime t_{disc} is shown in Fig. 4e. Aspect ratio $\delta = L/D$, where L is the thickness of a disc micelle, is also calculated. Note that L is governed by the length of A-block of the terpolymer. Hence in our study, the thickness of the disc micelles does not change as much as the diameter (Fig. S3).

A critical value exists at $D_c = 17.7$ DPD units and $\delta_c = L/D = 0.263$. Discs with D and δ near the critical values (open symbols, Fig. 4e and f) have t_{slow} (Group 2, slow transition). Most of the disc micelles with t_{fast} (filled symbols) have $D > D_c$ and $\delta < \delta_c$. These t_{fast} disc micelles are heavier and bigger than those with t_{slow} (see Fig. 5a). They also have a wider range of size (see Figs. 4e and 5a). The results suggest that once the micelles grow large enough, their merging process stops and they go through fast formation process into vesicles. This is because a smaller δ is likely to provide the necessary flexibility for these discs to transform to vesicle relatively easily. This is consistent with Huang et al. [35], which found that energy barrier for vesiculation decreased as planar membrane diameter increases. Together with a larger A , hence a higher surface energy, a large discs is less stable and hence shorter t_{disk} .

3.2. Effect of formation path on vesicle properties

Vesicles formed by disc micelles with t_{slow} and t_{fast} are denoted as $Vesicle_{slow}$ and $Vesicle_{fast}$ respectively.

3.2.1. Size and loading efficiency

Vesicles with controlled size are of practical use [36]. Understanding the relationship between vesicle size and loading efficiency is important. Vesicle loading efficiency, i.e. the amount of cargo a vesicle can encapsulate, is characterized by the number of cargo particles per

polymer chain making up the vesicle. Note that the cargo in this case is the solvent molecules encapsulated by a vesicle as a result of its formation. Both ABC-100 and ABC-125 give similar results. Since the number of polymer chains and the number of cargo are linked to the area and volume of the vesicle respectively, the loading efficiency increases linearly with the size of the vesicle (Fig. 5). This means $Vesicle_{slow}$, the smallest, lightest vesicles, have consistently lower loading efficiency than $Vesicle_{fast}$ (solid symbols, Fig. 5). This is contrary to result reported by Lohse [37] which showed an inverse relation between encapsulation efficiency and diameter of lipid vesicles.

3.2.2. Vesicle membrane permeability

Vesicle membrane permeability is characterized by the fraction of cargo remained in a vesicle f_{cargo} . The faster the reduction in f_{cargo} with time, the more permeable the membrane.

Typical findings are provided in Fig. 6. The permeability of a vesicle depends on its membrane bending rigidity k_C . k_C was calculated using equation $k_C = K_A h^2/24$, where K_A is the compressibility modulus and h is the membrane solvophobic thickness [35]. The compressibility modulus is calculated from area fluctuation of the membrane with $K_A = Ak_B T/\sigma_A^2$, where A is the area and σ_A is the mean-square fluctuation of the area [38]. When $k_C > 29k_B T$, f_{cargo} remains close to 1 (Fig. 6a1 – 6a3, 6b1 – 6b3), i.e. most of the cargo stayed in the vesicle. When $k_C < 29k_B T$, f_{cargo} drops with time (Fig. 6a4 – 6a6, 6b4 – 6b6), i.e. cargo leaks out of the vesicle. The lower k_C is, the faster f_{cargo} decreases.

$Vesicle_{slow}$ and $Vesicle_{fast}$ contain respectively 25% and 77.4% vesicles with $k_C > 29k_B T$. This suggests that the formation path have an effect on the bending rigidity, and the permeability of a vesicle. $Vesicle_{fast}$ tend to have higher bending rigidity, hence, low membrane permeability. In contrary, $Vesicle_{slow}$ are more likely to have lower bending rigidity and

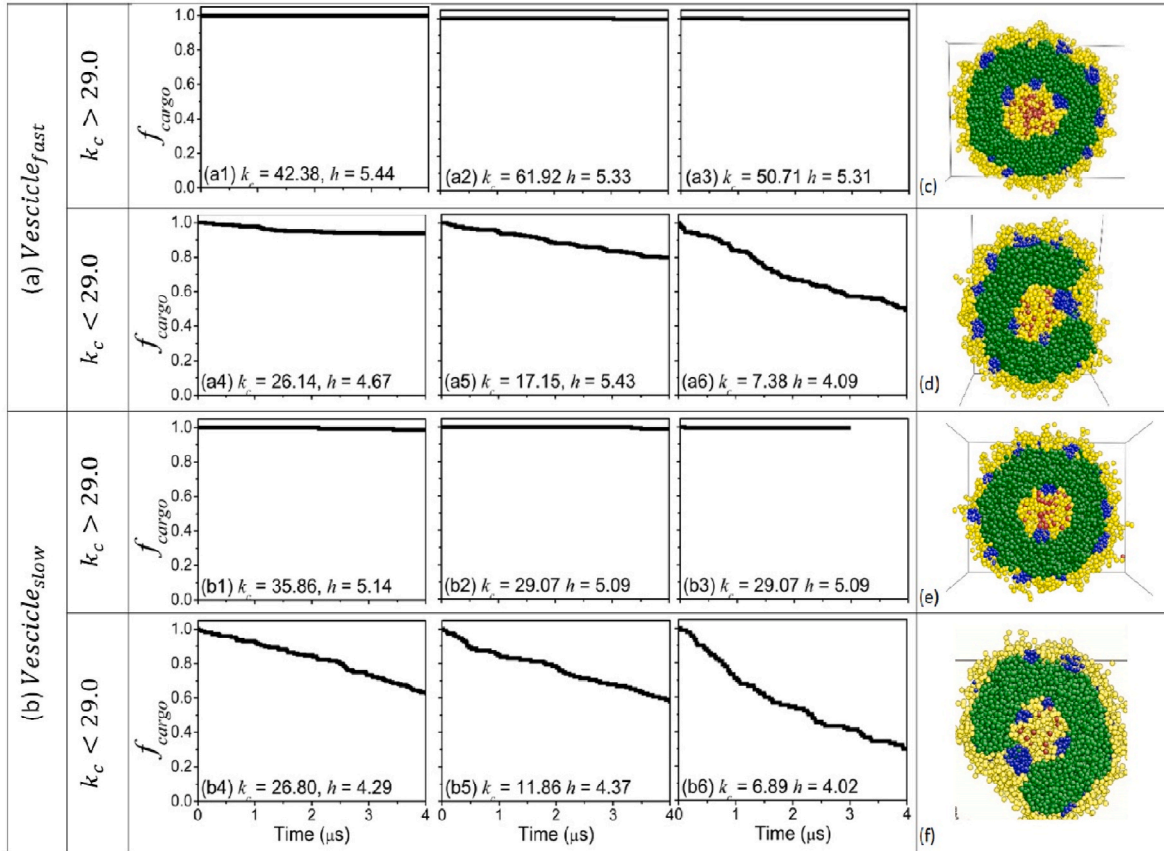


Fig. 6. The fraction of encapsulated cargo remained in a vesicle f_{cargo} for (a) $Vesicle_{fast}$ (vesicles formed with t_{fast}); (b) $Vesicle_{slow}$ (vesicles formed with t_{slow}); Cross sections typical of vesicles with (c) $Vesicle_{fast}$, high k_C ; (d) $Vesicle_{fast}$, low k_C ; (e) $Vesicle_{slow}$, high k_C ; and (f) $Vesicle_{slow}$, low k_C .

high membrane permeability.

Why the permeability differs with bending rigidity of a vesicle? The relationship between vesicle membrane thickness and bending rigidity were investigated (see Fig. S4) and there is no correlation. Studies on the influence of membrane thickness on its permeability give conflicting results [39,40] as its effect is likely to be chemistry specific.

Cross-sections of vesicles reveal morphological difference between low and high k_c vesicles (Fig. 6c–f). Membranes of high k_c vesicles (Fig. 6c and e) consist of solvophobic A-block inner leaflets (green), which separate the solvophilic inner and outer B-block solvated shells (yellow). The thickness of the membrane of a high k_c vesicle is homogeneous and the solvophilic cargo stay in its cavity. For low k_c vesicles (Fig. 6d and f), the inner and outer solvated shells (yellow) are connected at one point with a C-block domain (blue domain). The membrane surrounding this connection is thinner than the rest of the membrane. In our previous work, we show the importance of C-block connections, by providing thinner membrane in their surroundings and promoting the formation of solvophilic paths, a string of solvophilic B-beads that connects the inner and outer solvophilic shell, that facilitates cargo release [32]. Thus, we infer that solvophilic paths may form more readily with vesicles with low k_c , giving raise to quick cargo release.

3.3. Effect of shear on vesicle behavior

It is noted in Section 3.2 that in the absence of shear, vesicles with

high and low k_c have low and high cargo release rates respectively. This section, we would like to answer: how an application of shear affects the permeability of a vesicle? Here, the vesicle solutions experienced a shear rate of $1 \times 10^8 \text{ s}^{-1}$ and how f_{cargo} is affected is shown in Fig. 7. The cargo release rates of high k_c (>29) vesicles are not affected by the application of shear and remain low (Fig. 7a). Their membrane morphology also remains the same during shear. This could be ascribed to the high stiffness of the vesicle membrane, which makes them resistant to deformation (Fig. 7a4).

The cargo release rates of low k_c (<29) vesicles, however, are affected by bulk shear. The cargo release process of these vesicles can be divided into two stages. Upon shear, a sharp drop in f_{cargo} is observed at the very beginning (dash rectangles and insets in Fig. 7b). This is followed by a slow cargo release stage with a release rate similar to those of high k_c vesicles. Before the application of shear, the inner and outer solvated shells of these low k_c vesicles are connected by a C-block domain, as described in section 3.2.2 (and Fig. 6d and f). The slow cargo release rate observed coincides with a shear induced structural change (Fig. 7b4). The vesicle now has a membrane structure the same as those of high k_c (>29), with does not allow the easy formation of solvophilic path for cargo release rate.

4. Conclusion

The formation of polymeric vesicle via a disc wrap-up mechanism is

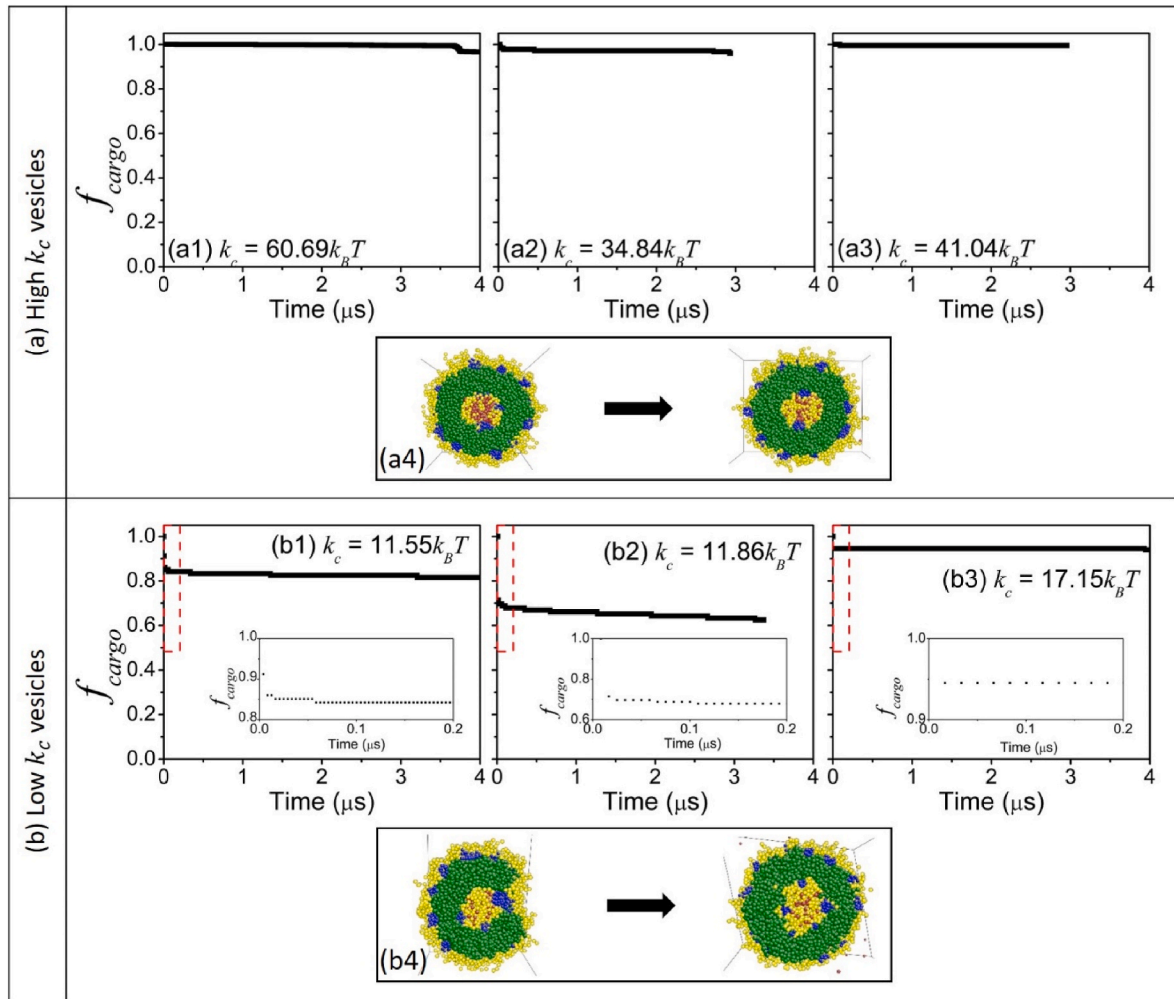


Fig. 7. How f_{cargo} changes with time under bulk shear for vesicles with (a) high bending rigidity and (b) low bending rigidity. (a4) and (b4) show vesicle structure before and after shear.

common under the bulk swelling process. Using raspberry vesicles formed by ABC terpolymers, we studied how the lifetime of a disc micelle before becoming a vesicle, t_{disc} , affects the properties of the resulting vesicle. The formation path has an effect on vesicle size, size distribution and loading efficiency.

Short t_{disc} discs micelles are more likely to form larger, stable, no-leak vesicles even though they will have larger size variations. These disc micelles consist of many chains and have diameters above a critical value of $D_c = 17.7$ DPD units. They possess a higher disk surface area and lower thickness to diameter ($\frac{t}{D}$) ratio. Thus, they are at a higher energy state and are more flexible. The resulting vesicles have higher loading efficiency. A large portion of these vesicles ($\sim 78\%$) have high membrane bending rigidity (k_C). These high k_C vesicles are very stable. They exhibit minimal cargo leaking with or without shear and the morphology of their vesicle membranes is unaffected by shear. The remaining low k_C vesicles have high permeability, with their membrane morphology favours the formation of a path allowing fast cargo release. When shear is applied, the morphology of these low k_C vesicles revert quickly to those of high k_C . This shear induced transition stops cargo leak.

Vesicles formed through long t_{disc} disc micelles have small size, narrow size distribution, low mass and low loading efficiency. Only a small fraction of these vesicles ($\sim 25\%$) have high k_C . Properties of high and low k_C vesicles are unaffected by t_{disc} of their originated disc micelles. Reducing the repulsion of the short solvophobic block of the terpolymer with the solvent hinders the formation of short t_{disc} discs.

Our results provide guidance on the selection of ABC raspberry vesicles as cargo carriers. To obtain vesicles with higher loading efficiency and lower permeability, one may use terpolymer with strong solvophobic block-solvent repulsion. Vesicles with more controllable size, higher permeability can be obtained by reducing solvophobic block-solvent repulsion.

CRediT authorship contribution statement

Y. Guo: Investigation, Software, Writing – original draft, Visualization. **L. di Mare:** Conceptualization, Supervision. **J.S.S. Wong:** Conceptualization, Supervision, Writing – review & editing.

Declaration of competing interest

The authors declare the following financial interests/personal relationships which may be considered as potential competing interests: Yingying Guo reports financial support was provided by Natural Science Foundation of Shandong Province.

Data availability

Data will be made available on request.

Acknowledgments

Y.G. is supported by the Natural Science Foundation of Shandong Province (No.ZR2021QE292). Results presented were produced using the High Performance Computing (HPC) facilities available at Imperial College Research Computing Service, <https://doi.org/10.14469/hp.c/2232>. For the purpose of open access, the authors have applied a Creative Commons Attribution(CC BY) license to any Author Accepted Manuscript version arising.

Appendix A. Supplementary data

Supplementary data to this article can be found online at <https://doi.org/10.1016/j.polymer.2023.126058>.

References

- [1] D.E. Discher, A. Eisenberg, Polymer vesicles, *Science* 297 (5583) (2002) 967–973.
- [2] F. Araste, A. Aliabadi, K. Abnous, S.M. Taghdisi, M. Ramezani, M. Alibolandi, Self-assembled polymeric vesicles: focus on polymersomes in cancer treatment, *J. Contr. Release* 330 (2021) 502–528.
- [3] C.G. Palivan, R. Goers, A. Najer, X.Y. Zhang, A. Car, W. Meier, Bioinspired polymer vesicles and membranes for biological and medical applications, *Chem. Soc. Rev.* 45 (2) (2016) 377–411.
- [4] X.-F. Xu, C.-Y. Pan, W.-J. Zhang, C.-Y. Hong, Polymerization-induced self-assembly generating vesicles with adjustable pH-responsive release performance, *Macromolecules* 52 (5) (2019) 1965–1975.
- [5] X. Wang, C. Yao, G. Zhang, S. Liu, Regulating vesicle bilayer permeability and selectivity via stimuli-triggered polymersome-to-PICs transition, *Nat. Commun.* 11 (1) (2020) 1–13.
- [6] O. Rifaie-Graham, N.F.B. Galensowske, C. Dean, J. Pollard, S. Balog, M.G. Gouveia, M. Chami, A. Vian, E. Amstad, M. Lattuada, N. Bruns, Shear stress-responsive polymersome nanoreactors inspired by the marine bioluminescence of dinoflagellates, *Angew. Chem., Int. Ed.* 60 (2) (2021) 904–909.
- [7] Y.-Q. Zhu, B. Yang, S. Chen, J.Z. Du, Polymer vesicles: mechanism, preparation, application, and responsive behavior, *Prog. Polym. Sci.* 64 (2017) 1–22.
- [8] X.R. Wang, C.Z. Yao, G.Y. Zhang, S.Y. Liu, Regulating vesicle bilayer permeability and selectivity via stimuli-triggered polymersome-to-PICs transition, *Nat. Commun.* 11 (1) (2020).
- [9] L. Qi, J. Qiao, Design of switchable enzyme carriers based on stimuli-responsive porous polymer membranes for bioapplications, *ACS Appl. Bio Mater.* 4 (6) (2021) 4706–4719.
- [10] M. Machtakova, S. Han, Y. Yangazoglu, I. Lieberwirth, H. Thérien-Aubin, K. Landfester, Self-sustaining enzyme nanocapsules perform on-site chemical reactions, *Nanoscale* 13 (7) (2021) 4051–4059.
- [11] F.H. Sobotta, M.T. Kuchenbrod, F.V. Gruschwitz, G. Festag, P. Bellstedt, S. Hoeppner, J.C. Brendel, Tuneable time delay in the burst release from oxidation-sensitive polymersomes made by PISA, *Angew. Chem. Int. Ed.* 60 (46) (2021) 24716–24723.
- [12] R. Rodriguez-Garcia, M. Mell, I. López-Montero, J. Netzel, T. Hellweg, F. Monroy, Polymersomes: smart vesicles of tunable rigidity and permeability, *Soft Matter* 7 (4) (2011) 1532–1542.
- [13] T. Nishimura, N. Sumi, Y. Koda, Y. Sasaki, K. Akiyoshi, Intrinsically permeable polymer vesicles based on carbohydrate-conjugated poly (2-oxazoline)s synthesized using a carbohydrate-based initiator system, *Polym. Chem.* 10 (6) (2019) 691–697.
- [14] S. Varlas, J.C. Foster, P.G. Georgiou, R. Keogh, J.T. Husband, D.S. Williams, R. K. O'Reilly, Tuning the membrane permeability of polymersome nanoreactors developed by aqueous emulsion polymerization-induced self-assembly, *Nanoscale* 11 (26) (2019) 12643–12654.
- [15] M. Kumar, M. Grzelakowski, J. Zilles, M. Clark, W. Meier, Highly permeable polymeric membranes based on the incorporation of the functional water channel protein Aquaporin Z, *P Natl Acad Sci USA* 104 (52) (2007) 20719–20724.
- [16] A.J. Kim, M.S. Kaucher, K.P. Davis, M. Peterca, M.R. Imam, N.A. Christian, D. H. Levine, F.S. Bates, V. Percec, D.A. Hammer, Proton transport from dendritic helical-pore-incorporated polymersomes, *Adv. Funct. Mater.* 19 (18) (2009) 2930–2936.
- [17] J. Kim, K.T. Kim, Polymersome-based modular nanoreactors with size-selective transmembrane permeability, *ACS Appl. Mater. Interfaces* 12 (20) (2020) 23502–23513.
- [18] S.J. Rijpkema, R. van Egeraat, W. Li, D.A. Wilson, Photo-cross-linking polymersome nanoreactors with size-selective permeability, *Macromolecules* 55 (13) (2022) 5744–5755.
- [19] N. Färber, J. Reitler, A. Kamenac, C. Westerhausen, Shear stress induced lipid order and permeability changes of giant unilamellar vesicles, *Biochim. Biophys. Acta Gen. Subj.* 1866 (10) (2022), 130199.
- [20] J. Du, S.P. Armes, Preparation of biocompatible zwitterionic block copolymer vesicles by direct dissolution in water and subsequent silicification within their membranes, *Langmuir* 25 (16) (2009) 9564–9570.
- [21] J. Du, S.P. Armes, Preparation of primary amine-based block copolymer vesicles by direct dissolution in water and subsequent stabilization by sol–gel chemistry, *Langmuir* 24 (23) (2008) 13710–13716.
- [22] J. Du, R.K. O'Reilly, Advances and challenges in smart and functional polymer vesicles, *Soft Matter* 5 (19) (2009) 3544–3561.
- [23] J. Rodriguez-Hernandez, F. Chécot, Y. Gnanou, S. Lecommandoux, Toward 'smart' nano-objects by self-assembly of block copolymers in solution, *Prog. Polym. Sci.* 30 (7) (2005) 691–724.
- [24] R. Bleul, R. Thiermann, M. Maskos, Techniques to control polymersome size, *Macromolecules* 48 (20) (2015) 7396–7409.
- [25] E.M. Ratamero, S.J. Royle, Calculating the maximum capacity of intracellular transport vesicles, *bioRxiv* (2019), 555813.
- [26] J.M. Zhang, J.H. Jiang, S. Lin, E.J. Cornel, C. Li, J.Z. Du, Polymersomes: from macromolecular self-assembly to particle assembly(dagger), *Chin. J. Chem.* 40 (15) (2022) 1842–1855.
- [27] W.C. Li, S.Q. Liu, H. Yao, G.X. Liao, Z.W. Si, X.J. Gong, L. Ren, L.G. Wang, Microparticle templating as a route to nanoscale polymer vesicles with controlled size distribution for anticancer drug delivery, *J. Colloid Interface Sci.* 508 (2017) 145–153.
- [28] M. Wu, Y.Y. Wang, Y.Y. Han, J. Cui, W. Jiang, A facile method for preparation of uniform polymeric vesicles with tunable size, *Nanoscale* 10 (31) (2018) 14860–14867.

- [29] Y.R. Wang, T.H. Yin, Z.W. Su, C. Qiu, Y. Wang, R.Q. Zheng, M.W. Chen, X.T. Shuai, Highly uniform ultrasound-sensitive nanospheres produced by a pH-induced micelle-to-vesicle transition for tumor-targeted drug delivery, *Nano Res.* 11 (7) (2018) 3710–3721.
- [30] M. Xiao, G. Xia, R. Wang, D. Xie, Controlling the self-assembly pathways of amphiphilic block copolymers into vesicles, *Soft Matter* 8 (30) (2012) 7865–7874.
- [31] C.J. Mable, N.J. Warren, K. Thompson, O. Mykhaylyk, S.P. Armes, Framboidal ABC triblock copolymer vesicles: a new class of efficient Pickering emulsifier, *Chem. Sci.* 6 (11) (2015) 6179–6188.
- [32] Y. Guo, L. Di Mare, R.K. Li, J.S. Wong, Cargo release from polymeric vesicles under shear, *Polymers* 10 (3) (2018) 336.
- [33] R.D. Groot, K. Rabone, Mesoscopic simulation of cell membrane damage, morphology change and rupture by nonionic surfactants, *Biophys. J.* 81 (2) (2001) 725–736.
- [34] Y.Y. Guo, Z.W. Ma, Z.J. Ding, R.K.Y. Li, Kinetics of laterally nanostructured vesicle formation by self-assembly of miktoarm star terpolymers in aqueous solution, *Langmuir* 29 (41) (2013) 12811–12817.
- [35] C.J. Huang, D. Quinn, Y. Sadovsky, S. Suresh, K.J. Hsia, Formation and size distribution of self-assembled vesicles, *P Natl Acad Sci USA* 114 (11) (2017) 2910–2915.
- [36] O. Diat, D. Roux, Preparation of monodisperse multilayer vesicles of controlled size and high encapsulation ratio, *J. Phys. II* 3 (1) (1993) 9–14.
- [37] B. Lohse, P.Y. Bolinger, D. Stamou, Encapsulation efficiency measured on single small unilamellar vesicles, *J. Am. Chem. Soc.* 130 (44) (2008) 14372–+.
- [38] Q. Waheed, O. Edholm, Undulation contributions to the area compressibility in lipid bilayer simulations, *Biophys. J.* 97 (10) (2009) 2754–2760.
- [39] Z. Bai, B. Zhao, T.P. Lodge, Bilayer membrane permeability of ionic liquid-filled block copolymer vesicles in aqueous solution, *J. Phys. Chem. B* 116 (28) (2012) 8282–8289.
- [40] J.C. Mathai, S. Tristram-Nagle, J.F. Nagle, M.L. Zeidel, Structural determinants of water permeability through the lipid membrane, *J. Gen. Physiol.* 131 (1) (2008) 69–76.